NASA Contractor Report 3284

Wake Characteristics of Buildings in Disturbed Boundary Layers

Earl Logan, Jr., and Jingfa Chang

CONTRACT NAS8-32357
MAY 1980

NASA

NASA Contractor Report 3284

Wake Characteristics of Buildings in Disturbed Boundary Layers

Earl Logan, Jr., and Jingfa Chang
Arizona State University
Tempe, Arizona

Prepared for
Marshall Space Flight Center
under Contract NAS8-32357

National Aeronautics
and Space Administration

**Scientific and Technical
Information Office**

1980

AUTHORS' ACKNOWLEDGMENTS

The work reported herein was supported by the National Aeronautics and Space Administration, Marshall Space Flight Center, Space Sciences Laboratory, Atmospheric Sciences Division, under Contract No. NAS8-32357.

The authors are indebted to Messrs. John H. Enders, Solomon Weiss, and A. Richard Tobiason of Aviation Safety, Office of Aeronautics and Space Technology (OAST), NASA Headquarters, Washington, D.C., for their support of this research. Special thanks also go to Mr. Dennis W. Camp and Mrs. Margaret B. Alexander of the Atmospheric Sciences Division, Space Sciences Laboratory, NASA/Marshall Space Flight Center, who were the scientific monitors of the program.

FOREWORD

This study was initiated to determine the feasibility of predicting wake profiles behind buildings and natural obstacles using a scaled model in a wind tunnel. The wind tunnel approach is preferable because of economy of time and money, simplicity and convenience. This is the second report of a continuing program sponsored by the Fluid Dynamics Branch, Atmospheric Sciences Division of the Space Sciences Laboratory at the George C. Marshall Space Flight Center, National Aeronautics and Space Administration, Huntsville, Alabama.

This research was conducted under the technical direction of Mr. Dennis W. Camp and Mrs. Margaret Alexander of the Space Sciences Laboratory at Marshall Space Flight Center. The support for this research was provided by Mr. John Enders of the Aeronautical Operating Systems Division, Office of Advanced Research and Technology, NASA Headquarters.

TABLE OF CONTENTS

LIST OF TABLES

LIST OF FIGURES

NOMENCLATURE

A,B	Constants in Equation (9)
D	Tube diameter (inside)
H	Height of roughness element (obstacle)
k	von Karman constant
MOM	Momentum flow per unit width
n	Power law exponent
R	Tube radius (inside)
S	Spacing between roughness elements (obstacles)
T1,T2,T3,T4,T5,T6	meteorological towers Nos. 1,2,3,4,5,6
u^*	Friction velocity for fully-developed flow
u'	RMS value of longitudinal fluctuations
$\overline{uv}$	Axial component of Reynold shear stress
U	Axial component of mean velocity
U_c	Mean velocity at pipe centerline
U_o	Mean velocity at pipe centerline upstream of first element
U_r	horizontal component of air velocity far upstream of building (T1) at z/H = 6.5
U_∞	geostrophic or free stream wind velocity
ΔU	velocity deficit based on upstream velocity
v'	RMS value of radial fluctuations

W	Width of roughness element
w'	RMS value of circumferential fluctuations
x	Axial coordinate measured from downstream side of element
y	Wall distance measured from tube wall
z	elevation above ground (or wall distance y)
z_o	roughness length
δ	model or prototype boundary layer thickness
δ_i	Internal boundary layer thickness

CHAPTER 1

INTRODUCTION

The motivation for the work described in this report derives from the need to understand the wind environment around air terminals. Ascent or descent of aircraft through the atmospheric boundary layer is accompanied by changes in lift associated with changes in wind speed with altitude. The acceleration produced by the brief action of unbalanced forces results in deviations from the original flight path for descending flight. The above effect is enhanced by induced flows produced by buildings or natural obstacles in the vicinity of airports. The effect of these surface obstacles on the aerospace environment around airports has been reviewed recently by Fichtl, et al. [1]. Shear layers, or wakes, produced downwind of surface obstacles can prove hazardous to aircraft, especially those of the V/STOL type, because of the high rate of change of wind speed with altitude in the layer. Clearly research is needed to determine the locations of these regions of induced flows in the wakes of surface obstacles and their effects on aeronautical systems.

Sources of hazardous low-level wind conditions around airports have been discussed by Fichtl, Camp and Frost (1977). Wakes from bluff bodies, such as buildings, are among the sources mentioned. This is especially true of STOL vehicles landing or taking off over buildings, fences or other obstacles. Research which can predict

the extent and severity of wind speed change is currently needed.

Experimental work undertaken at NASA Marshall Space Flight Center has been reported by Frost and Shahabi (1977) and by Frost, et al. (1977). This work involved the use of instrumented wind towers to study the wake of a simulated block building 3.2-m high by 26.8-m long under field conditions. Figure 1 shows the arrangement of towers used in this study. Data of principal interest were taken when the wind direction was from towers T1 to T6. Mean horizontal and turbulence profiles were determined from readings of anemometers located at heights z of 3, 6.2, 12 and 20.88 m above the ground.

The velocity and turbulence profiles measured in the field have been compared with wind tunnel profiles in the wake of a 1/50-scale model of the 3.2 x 2.4 x 26.8-m building depicted in Fig. 1. The results of the model study were reported by Woo, Peterka and Cermak (1977), and a preliminary comparison of data was presented by Logan and Camp (1978).

A comparison of typical field (Run No. 8504) and wind tunnel profiles from the above studies is shown in Fig. 2. If the velocity profiles are represented by the power law

$$\frac{U}{U_\infty} = \left(\frac{z}{\delta}\right)^n \qquad (1)$$

then the exponent n corresponding to the upstream profile has a value of 0.26 for the field data and 0.27 for the wind tunnel data. Although

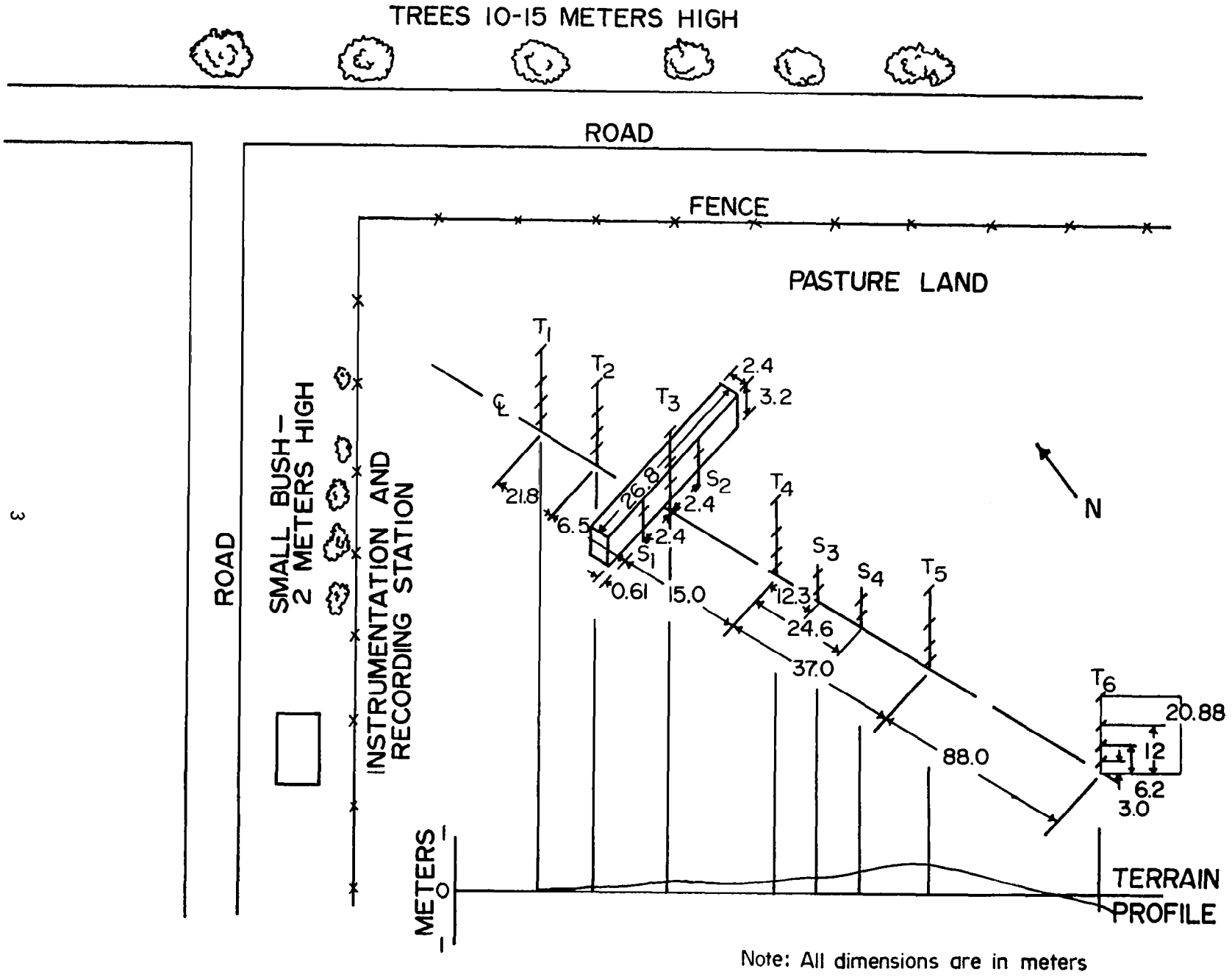

Fig. 1 Tower Arrangement in Field Study (Frost, et al., 1977)

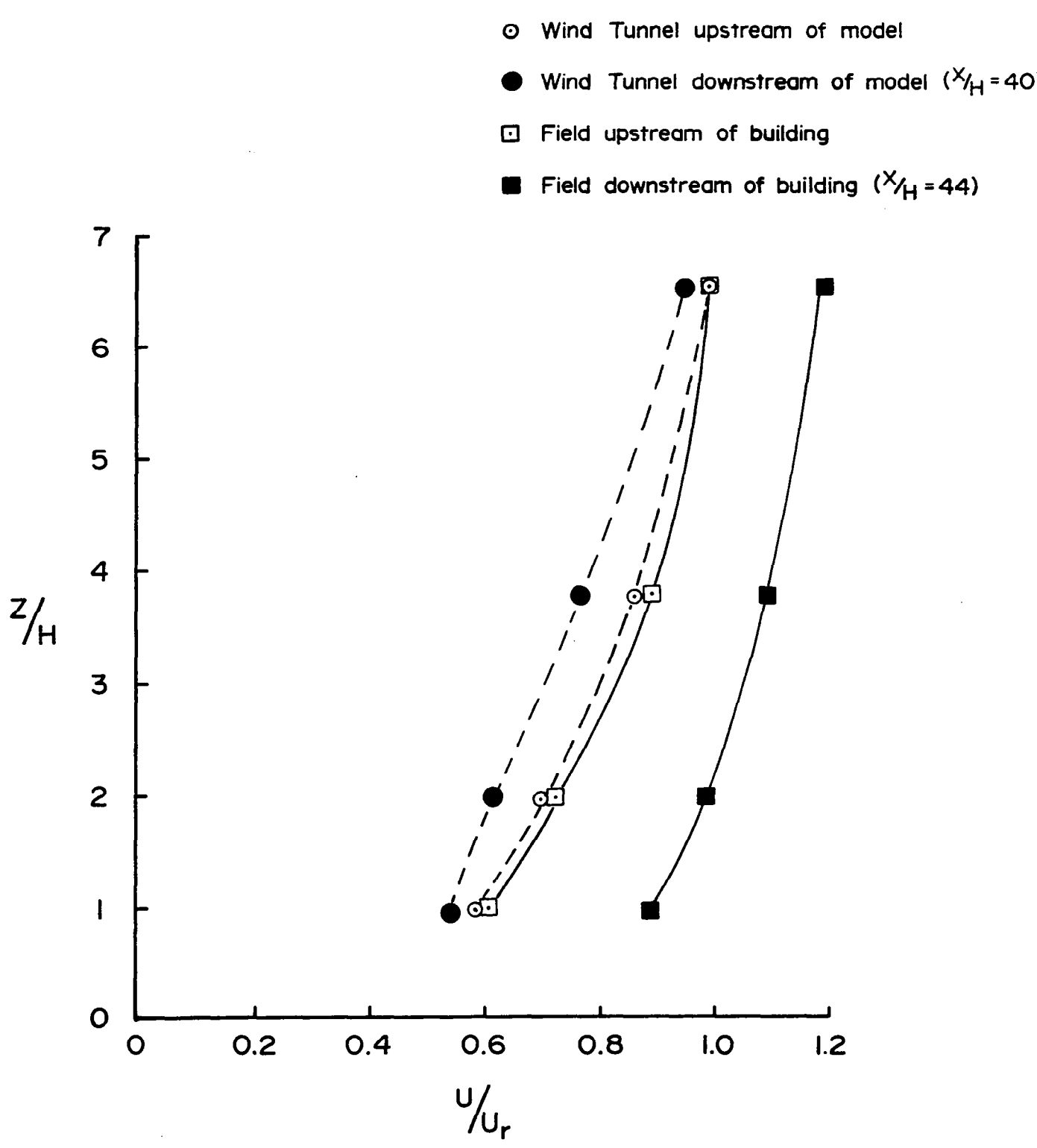

Fig. 2 Comparison of Field and Wind Tunnel Data (Woo, et al., 1977)

the profiles for model and prototype are very similar upstream of the obstacle, their downstream profiles are quite different. The model wake profile shows a retardation, or momentum loss, while the prototype wake profile indicates an acceleration, or momentum gain. A difference in power law exponent n is also noted; the model wake has a value near its original value, while the prototype wake has an exponent of 0.148, a much lower value.

The momentum gain indicated in Fig. 2 has been quantified for several runs and the momentum flow (MOM) for each station is listed in Table 1. The quantity MOM is defined as

$$MOM = \int_0^{20.88} U^2 dz \quad . \tag{2}$$

In every case the field data show an increase in momentum, e.g., there is a 59% increase for Run No. 8504. In contrast, the wind tunnel profile shows an 18% decrease of momentum at approximately the same downstream station (x/H = 40, H = height of model or building). This is the expected result for flow over an obstacle; thus a rational explanation of the momentum rise must be sought.

In view of the preceding data, coupled with the fact that roughness length z_o calculated from the logarithmic relation,

$$z_o = \frac{z}{\exp \frac{KU}{u^*}} \tag{3}$$

is unreasonably high at station T1, Logan and Camp (1978) hypothesized

TABLE 1. MOMENTUM INTEGRAL EVALUATION
(UNITS ARE M^3/S^2)

RUN NO.	MOM AT T1	MOM AT T6	% INCREASE
8501	554	916	65
8502	660	919	39
8503	650	1007	55
8504	629	998	59
8512	421	617	47
8407	334	428	28
8408	288	410	42

that the wind profile at T1 is a non-equilibrium profile, whereas the upstream wind tunnel profile is an equilibrium profile. The building wake profile shown in Fig. 2 corresponds to a roughness length z_o of 0.0107 m, which is a reasonable value for the terrain at the site of the experiments. The change in profile from T1 to T6 may then be an adjustment from a non-equilibrium, or disturbed condition, to a near-equilibrium condition at T6. It is suggested that such a non-equilibrium state could have been created by obstacles upwind of the building, viz., trees, fences, bushes, etc., as could be inferred from Fig. 1. To test this hypothesis qualitatively an experiment was conducted in an existing operating facilty--a pipe flow apparatus.

CHAPTER 2

FLOW FACILITY

Figure 3 shows the apparatus used for the current experiments involving a disturbed boundary layer which encounters an obstacle. An air flow is created in a 3.97-inch (100.8 mm) diameter aluminum pipe at a Reynolds number, defined as centerline velocity U_c times pipe diameter over air kinematic viscosity, of 50,000. The pipe is of sufficient length to produce a fully developed equilibrium flow which is then disturbed by a ring-type roughness element located in a 4-inch diameter, plastic tube connected to the end of the aluminum pipe. As shown in Fig. 4, a second roughness element is installed a distance S downstream of the first and serves to simulate the building in a disturbed boundary layer. Wake profiles are measured at several stations a distance x from the rear side of the second roughness element. Each element is rectangular in cross section having a width w = 0.1574 inches (5.0 mm) and a height H = 0.2098 inches (5.33 mm). The spacing S between the elements is varied, so that the dimensionless ratio S/H has values of 30, 60, 120 and 240, which ensures wide variation of the power law exponent of the disturbed profile just upstream of the second element.

The constant-temperature hot-wire anemometer was used to determine mean and fluctuating velocities. Probes were held in the traversing device and moved longitudinally and radially to the desired

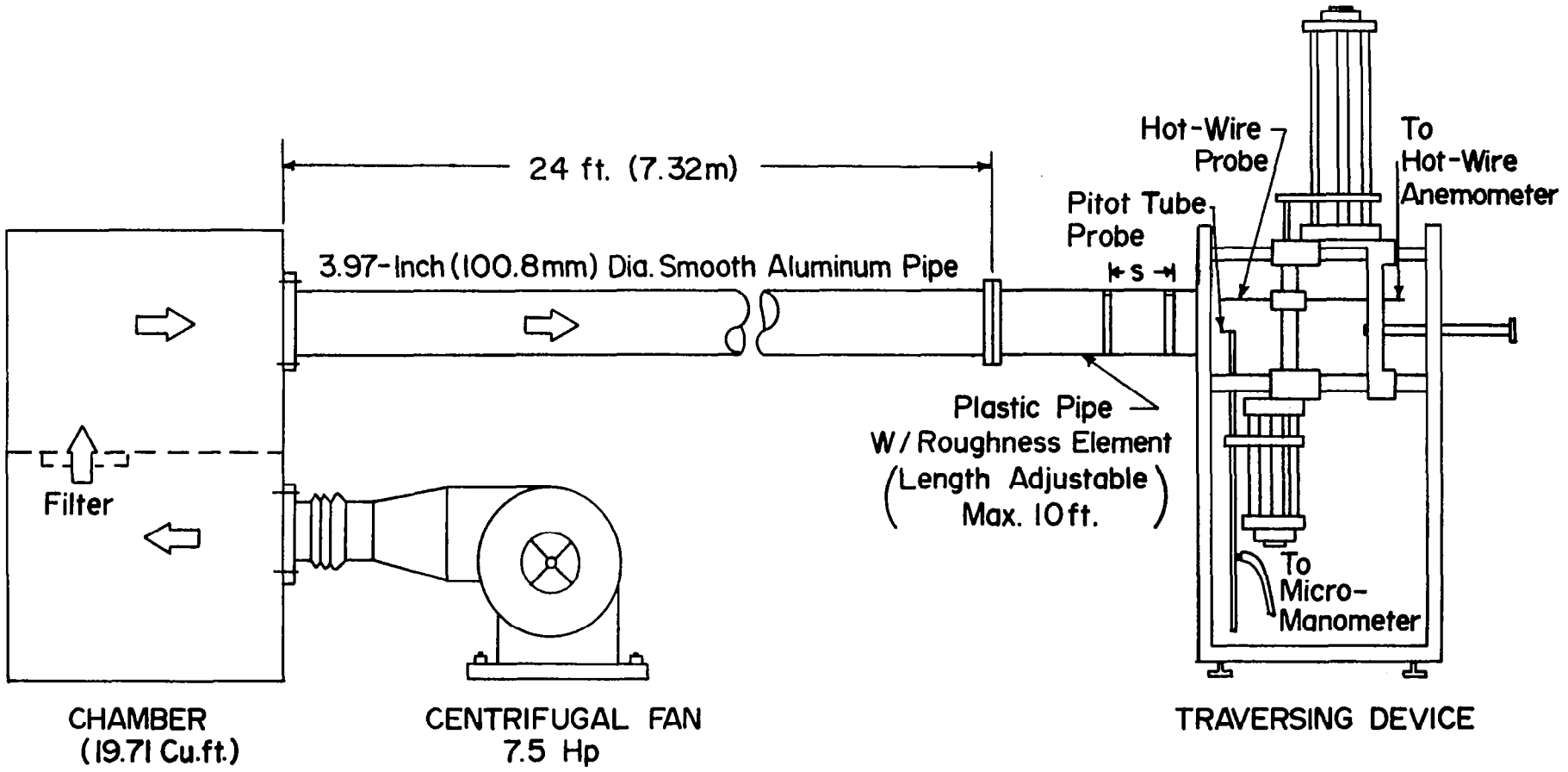

Fig. 3 Pipe Flow Facility

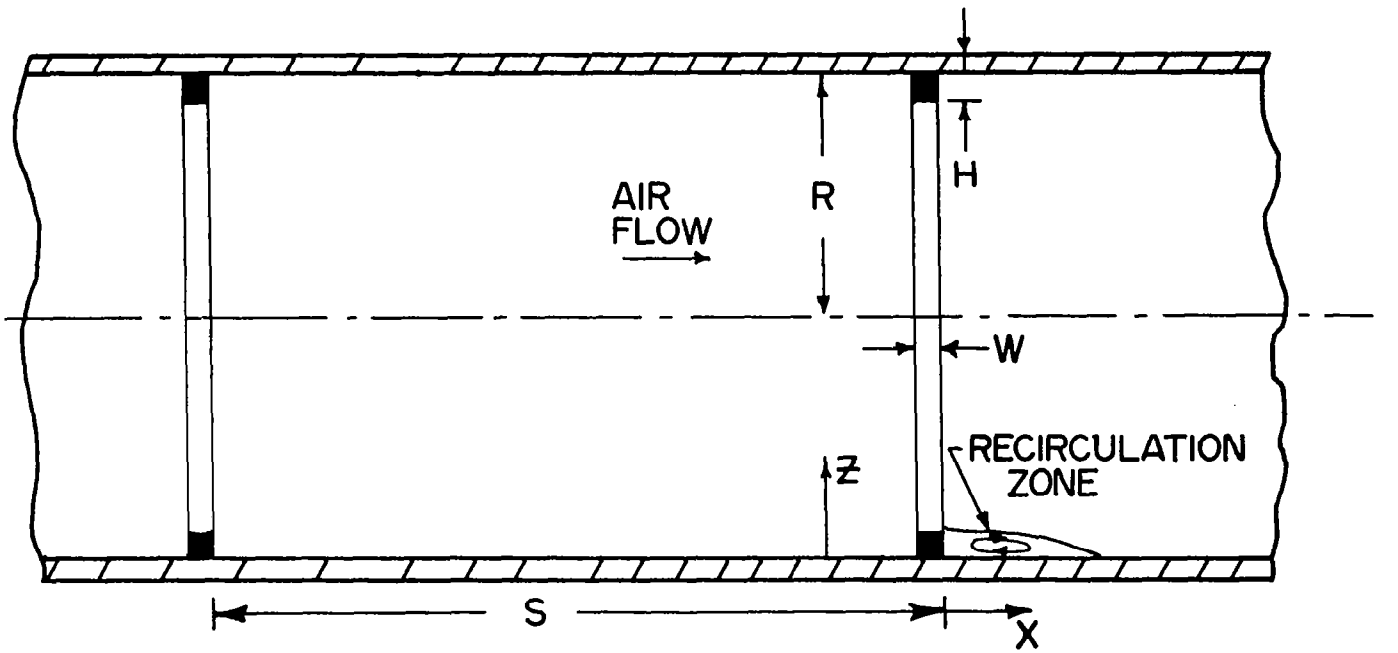

Fig. 4 Arrangement of Roughness Elements

dimensionless wall distance y/R and downstream distance x/H. The normal wire probes (DISA 55P11) were calibrated with a standard 0.065-inch (1.65 mm) diameter pitot tube. Preliminary measurements of fully developed profiles were compared with those of Laufer (1954) and found to be in good agreement. The wall shear stress, determined from static pressure drop, was compared with the extrapolated value of Reynolds shear stress, determined from slant wire measurements, and found to be in good agreement. The measured shear stress distribution was linear with a value of zero at the centerline. The above procedures served as a check on the reliability of the data procured from the experimental facility and presented in the following sections.

CHAPTER 3

OBSTACLE IN AN EQUILIBRIUM LAYER

Measurements of mean velocity U have been taken upstream of a single roughness element at stations x/H = -12, -10, -8, -6, -4, -2, -1.5 and -1, where x is longitudinal distance measured from the downstream edge of the element with a positive sign indicating the flow direction. The measurements show a decrease in velocity near the wall as the obstacle is approached, accompanied by an acceleration in the region farther from the wall. Figure 5 shows this effect at x/H = -8, the approximate non-dimensional location of Tower T1 in Fig. 1. The velocity U is non-dimensionalized with the centerline velocity U_0 for the fully developed profile, and the distance z from the pipe wall is non-dimensionalized with the element height H. The retardation at z/H = 0.4 amounts to 6% of the upstream value. This is in qualitative agreement with the field measurements of Rider (1952) which indicate a 5% retardation upwind of a hedge at the same values of z/H and x/H. Rider's data indicate zero retaration at about z/H = 2.6 and x/H = -8, and the data of Fig. 5 show zero retardation at roughly the same position. At higher elevations the streamlines are forced together, and acceleration of air around the obstacle results. The latter effect will be greatest just above the roughness element but will diminish with increasing downstream distance x. However, the predominant downstream effect must be a retardation characterized by

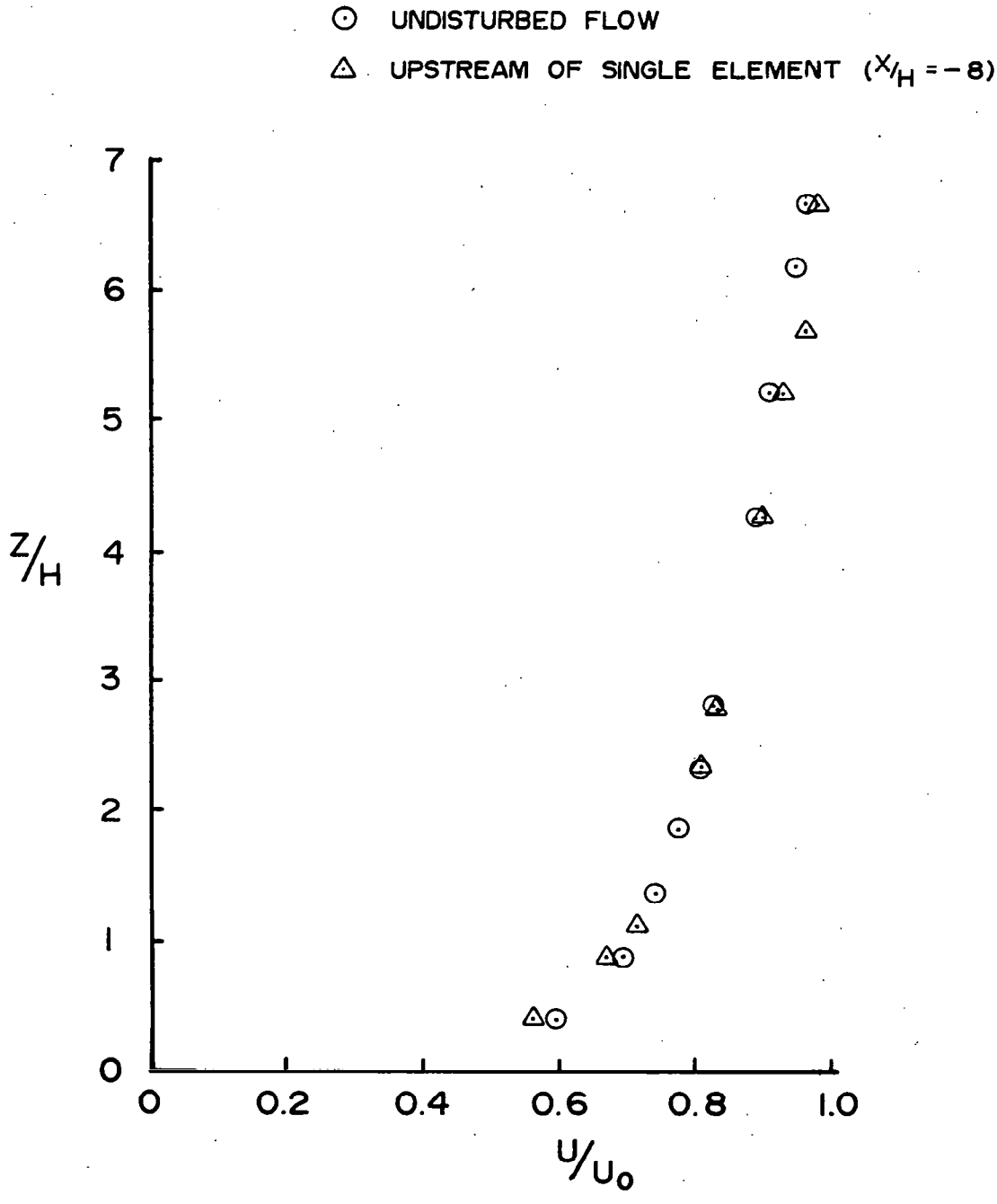

Fig. 5 Effect of Obstacle on Upstream Flow

a velocity or momentum deficit proportional to the drag force on the roughness element.

The velocity profiles in the wake of the single element at stations x/H = 5, 16.4 and 40 are shown in Fig. 6. Using the upstream profile at x/H = -8 for comparison, it is seen that a strong deceleration occurs at x/H = 5 and that the affected region grows in the direction away from the wall, as indicated by profiles at x/H = 16.4 and 40. The momentum flow can be quantified by redefining the integral MOM as

$$MOM = \int_{r/H}^{9.533} (U/U_o)^2 \, d(r/H)^2 \qquad (4)$$

where the lower limit is r/H at any z/H and the upper limit is r/H at z/H = 0 and r denotes the radial coordinate. If the lower limit is set at an r/H value corresponding to z/H = 2.3, then MOM = 17.6 at x/H = -8, 11.7 at x/H = 5, 12.6 at x/H = 16.4 and 15.7 at x/H = 40. Thus the value of MOM taken between any limits tends to return to the upstream equilibrium value. If the upstream values of MOM are based on a non-equilibrium profile, such as those to be presented in the next section, then MOM will not tend to return to them but, instead, to the values of MOM found far upstream in an equilibrium layer.

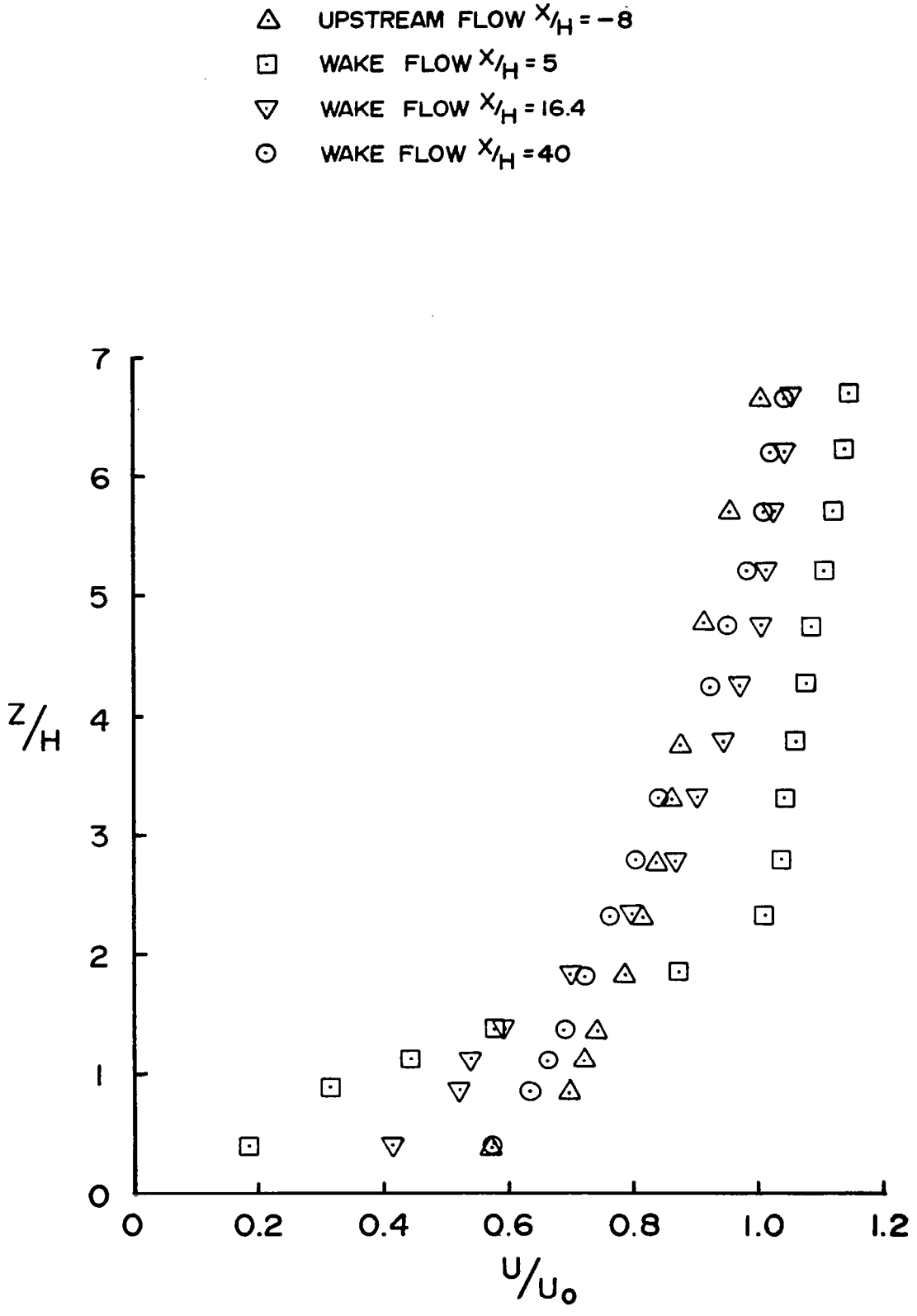

Fig. 6 Wake Profiles for the Isolated Obstacle

CHAPTER 4

OBSTACLE IN A DISTURBED LAYER

Figure 7 shows the results of four spacings used in the experiments. The solid circles indicate the upstream velocity profile for the spacing s/H = 30. This spacing gives a profile at x/H = -8 with respect to the second element (or x/H = 22 with respect to the first element), which has a power law exponent n = 0.381. Wider spacings of 60, 120 and 240 result in exponents of 0.23, 0.144 and 0.144, respectively, for the upstream profile. Apparent values of z_0/H, determined from (3), are 0.1466, 0.0272, 0.0019 and 0.0037 for s/H = 30, 60, 120 and ∞, respectively.

The upstream profiles produced at the four distances downstream of the first obstacle are shown in contrast to the fully developed, or equilibrium, profile (dashed line). The wake profiles behind the second element must eventually return to the form indicated by the dashed line in Figure 7. Thus for each upstream profile a velocity deficit exists up to some z/H level. As may be observed in Fig. 7, there must be a velocity excess in the core region of the pipe flow, so that mass is conserved; i.e.,

$$\int_0^{9.533} (U/U_0)\, d(r/H)^2 = \text{constant.} \qquad (5)$$

The integral in (5) was evaluated numerically, and the ratio U_c/U_0 for each x/H station was corrected slightly to assure constancy

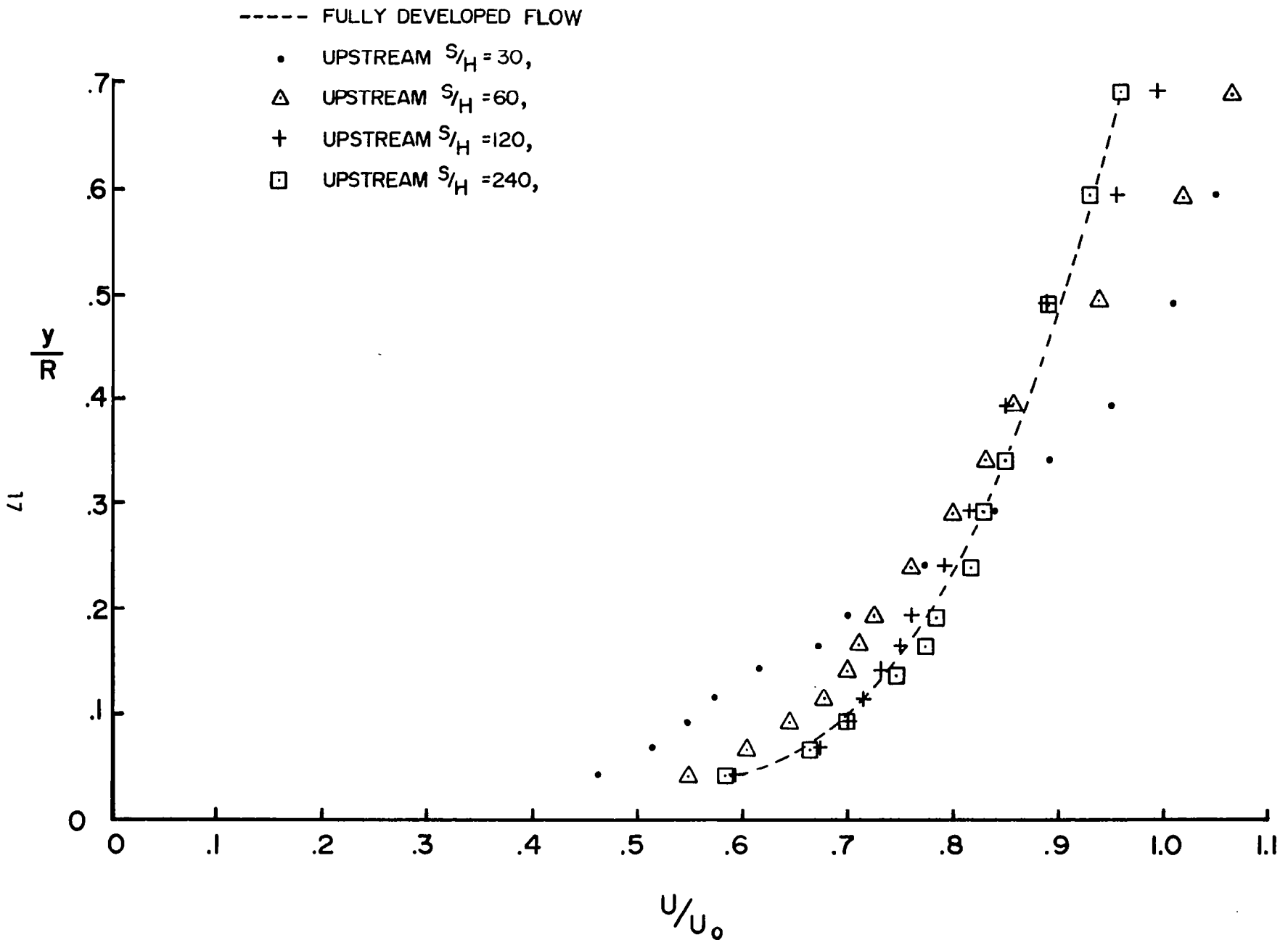

Fig. 7 Effect of Spacing on Upstream Profiles

of mass flow in the profiles of Figure 7 (U_c denotes local centerline velocity; U_o denotes centerline velocity for fully developed flow). Equation (4) was then applied to evaluate numerically the momentum flow upstream from the data of Figure 7 as well as downstream for similar profiles at stations x/H = 4.88, 16.44 and 35. The difference in momentum ΔMOM, defined by the difference

$$\Delta MOM = MOM\ (x/H) - MOM\ (x/H = -8), \tag{6}$$

was calculated and plotted in Figure 8. The curves in this figure show ΔMOM for the single element with an equilibrium upstream layer for integration from the wall to z/H = 1.2 (upper curve) and z/H = 2.3 (lower curve). The effect on the non-equilibrium upstream layers is shown by means of the circular, triangular and square points. The data of Fig. 8 show that the ΔMOM curves shift upward as the power law exponent n of the upstream profile is increased. This relationship is crudely approximated for the case of the z/H = 1.1 data of Figure 8 by

$$\Delta MOM\Big|_{1.1} = 0.48\ (x/H)^{0.7} - 8.5 + 10n\ . \tag{7}$$

Equation (7) predicts qualitatively the upward shifting of the points in Figure 8 with a higher n (or lower s/H). Clearly ΔMOM will achieve positive values at smaller values of x/H for higher values of n; e.g., beyond x/H = 22 a curve through the open circles would have positive values of ΔMOM.

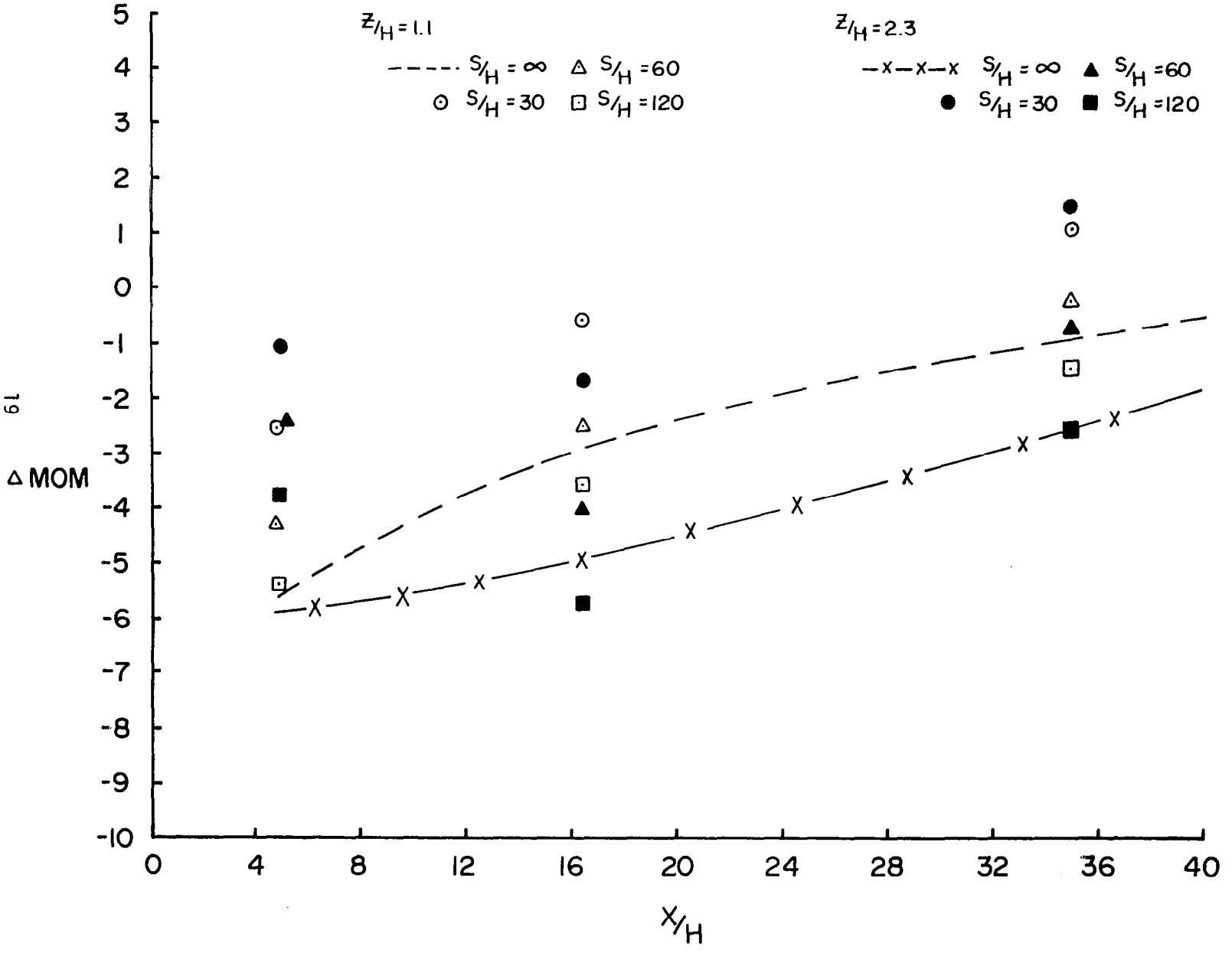

Fig. 8 Momentum Flow Deficit in Obstacle's Wake

The curve for the parameter r/H (or z/H), which is the limit on the integral MOM, asymptotically approaches a fixed, or limiting, value ΔMOM_{LIM} given by

$$\Delta MOM_{LIM} = MOM(\infty) - MOM(-8) \qquad (8)$$

i.e., the value of MOM for the fully developed flow minus MOM upstream at x/H = -8. Some limiting values are tabulated in Table 2. Quantities in parentheses express ΔMOM as a percentage of the upstream value of MOM.

As z/H is increased, ΔMOM_{LIM} is increased and then decreased. The decrease is associated with the excess of momentum found in the core region (z/H > 3) upstream of the obstacle, as depicted in Figure 7. The latter effect is much larger in pipe flow than in the unconfined flow reported in the field studies and should not be considered in making comparisons. Little effect is observed for S/H = 120, 240 and ∞, since the power law exponents of profiles at these stations, viz., 0.144, 0.144, and 0.156, respectively, are very close to the value of n for fully developed flow, viz., 0.159. On the other hand, a significant rise in MOM is observed for spacings of S/H = 30 and 60 in the wall region of the pipe flow.

The data presented in Figures 7 and 8 and Table 2 demonstrate the effect observed in the field, viz., an apparent increase in momentum flow (MOM) as determined by integration over the lower part of the layer. The percent increase of MOM observed in the wall region (z/H < 3) of the pipe flow (Table 2) is in qualitative agreement with those calculated from the field data (Table 1).

TABLE 2

LIMITING VALUES OF MOMENTUM FLOW DIFFERENCE

(ΔMOM_{LIM})

Upper Limit z/H	s/H = 30	60	120	240	∞
1.1	2.6(61)	.9(15)	-0.1(2)	-0.1(1)	0.2(4)
2.3	4.9(38)	2.2(14)	0.1(1)	-0.5(2)	0.3(2)
3.8	4.2(15)	3.1(11)	0.6(2)	-0.4(1)	0.4(1)
4.7	2.3(6)	2.8(8)	0.8(2)	-0.2(1)	0.5(1)
5.7	0.5(1)	1.9(4)	0.8(2)	-0.1(.1)	0.4(1)

CHAPTER 5

TURBULENCE

The rms of the longitudinal component u' of the turbulence was measured at stations ahead of and behind the second roughness element. Upstream profiles of u', non-dimensionalized with the friction velocity u*, are depicted in Fig. 9 for each roughness element spacing. The fully developed profile is shown as a dashed curve. All of the non-equilibrium profiles must approach the equilibrium (dashed curve) profile as x/H is increased.

The variation of u'/u* with x/H is shown in Table 3 for two values of z/H. In this table the quantities in parentheses are ratios of downstream to upstream turbulence. The influence of the form of the upstream profile, i.e., the power law exponent, is clearly seen from the tabulated data. As n increases, i.e., as s/H decreases, the relative turbulence level at a given station decreases. Table 3 shows that the magnitude of the rise in turbulence at x/H = 4.88 is related more to the turbulence level at x/H = -8 than to the level at x/H = 4.88. Thus the upstream turbulence energy is related to the profile shape; e.g., it is considerably greater for s/H = 30 (n = 0.381) than for s/H = 60 (n = 0.23), which means that the percentage rise in turbulence intensity is smaller for s/H = 30 than for s/H = 60. This result is in qualitative agreement with the observation made by Logan and Camp (1978) that a much smaller relative turbu-

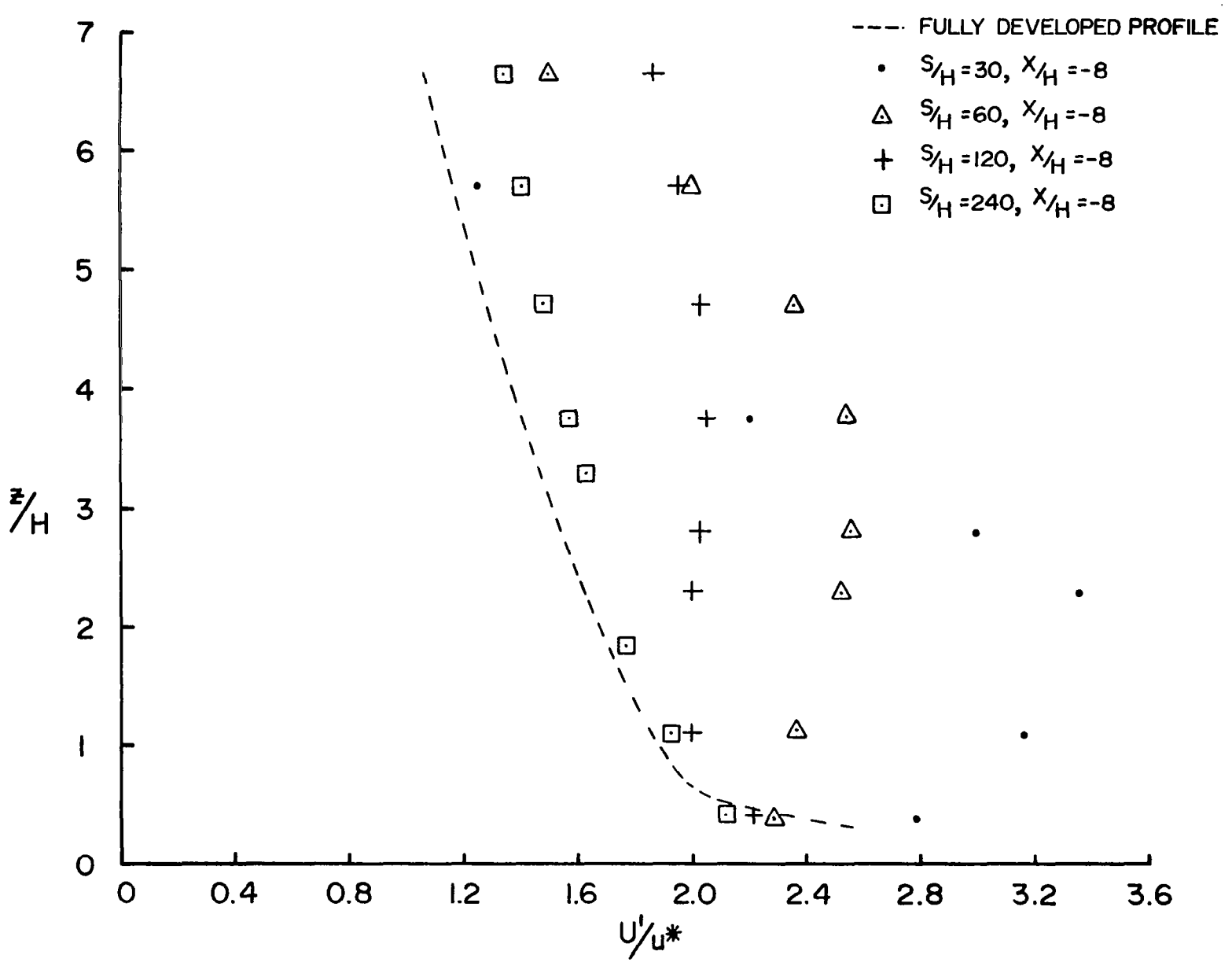

Fig. 9 Effect of Spacing on Upstream Turbulence

TABLE 3

TURBULENCE IN WAKE (u'/u^*)

		x/H			
Z/H	S/H	-8	4.88	16.44	35
1.1	30	3.15	5.55(1.76)	4.13(1.31)	2.99(0.95)
1.1	60	2.36	5.75(2.44)	4.25(1.80)	2.99(1.27)
1.1	120	1.99	5.59(2.81)	4.10(2.06)	2.87(1.44)
1.1	∞	1.81	5.12(2.83)	4.02(2.22)	2.95(1.63)
2.3	30	3.35	3.39(1.01)	4.41(1.32)	3.39(1.01)
2.3	60	2.52	2.54(1.01)	4.25(1.69)	3.31(1.31)
2.3	120	2.01	2.09(1.04)	3.90(1.94)	3.07(1.53)
2.3	∞	1.64	2.21(1.34)	3.43(2.09)	3.07(1.87)

lence excess occurred in the prototype (non-equilibrium) wake than occurred in the model (equilibrium) wake. It should be noted that the data of Table 3 indicate a very slow return to an equilibrium profile; e.g., at $x/H = 35$, $s/H = 30$, the turbulence level is approximately that at $x/H = -8$, which is roughly double the equilibrium value. The rate of decay of turbulence level does not appear to be a strong function of n.

CHAPTER 6

SMOOTH-ROUGH TRANSITION

The present measurements can be interpreted as a study of the first stage in the adjustment of a smooth-wall pipe flow to repeated-rib roughness elements. The smooth-rough transition has been studied by Siuru and Logan (1977), and the response of the flow to a single ring-type element was investigated by Phataraphruk and Logan (1978, 1979). The single element produces an internal boundary layer which grows as in the repeated-roughness geometry but is accompanied by a rise and fall of mean velocity deficit and turbulence intensity excess with respect to fully developed, smooth-wall values. The present work extends the above-mentioned research to include the effect of an upstream element on the wake of a second element. For artificially roughened pipes, the flow situation reported for the second element is somewhat similar to that for all widely spaced roughness elements downstream of the first; i.e., the flow approaching a given element has been disturbed by the element just upstream. The present results would not be relevant to closely spaced elements for which reattachment does not occur.

Typical mean velocity profiles are shown in Figs. 10 and 11. In these figures the wall distance is plotted on a logarithmic scale and non-dimensionalized with the inside radius of the plastic tube. Mean velocity is non-dimensionalized with its centerline value. The same scale of U/U_c applies to all profiles when its zero point is

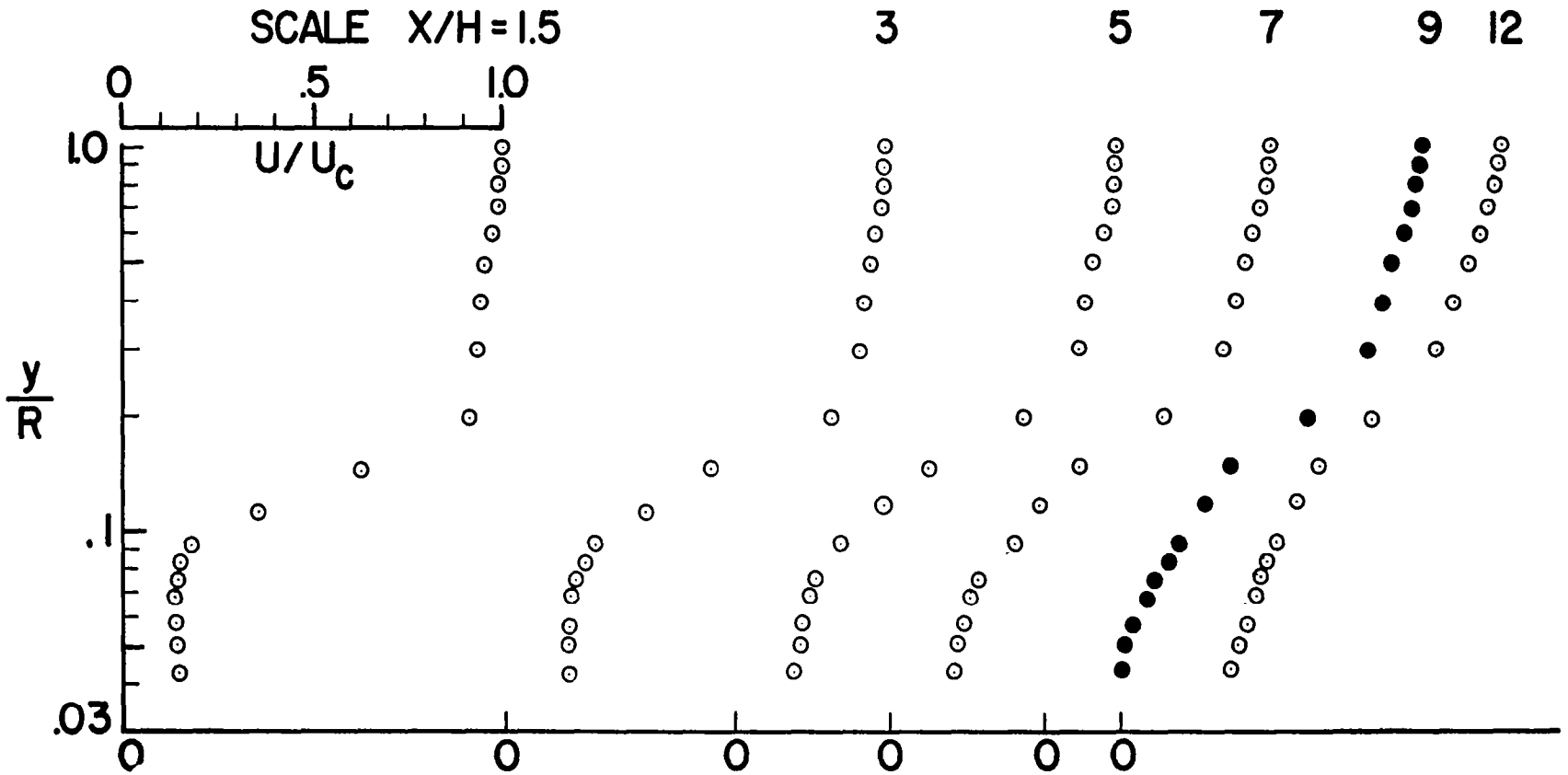

Fig. 10 Mean Velocity Profiles for S/H = ∞

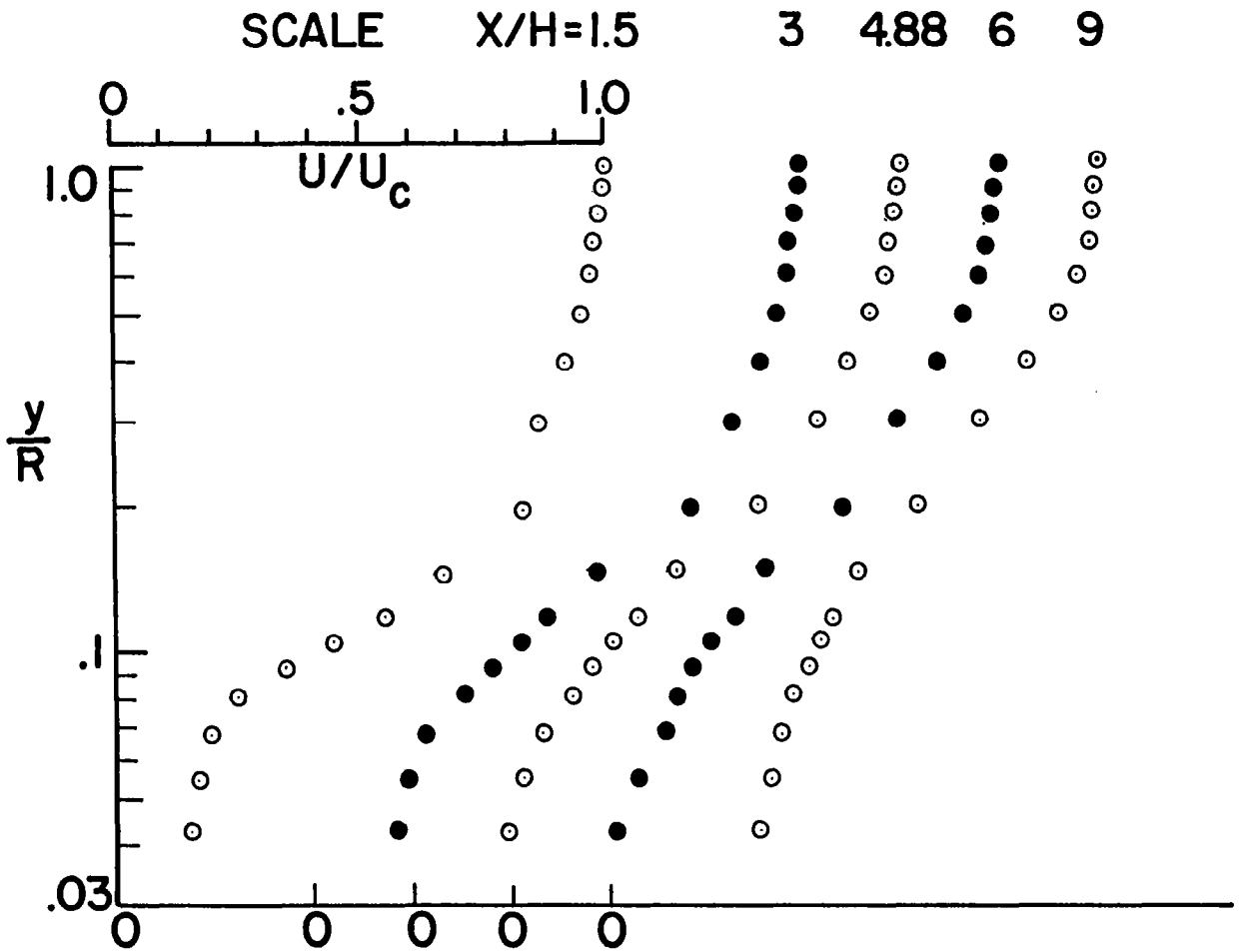

Fig. 11 Mean Velocity Profiles for S/H = 30

aligned with the zero marked on the horizontal axis. The downstream distance x is measured from the rear face of the second element.

The profiles of Figs. 10 and 11 show bends, which have been called "knees," below which the fluid has been retarded by the obstacle. Further downstream it is noted that the knee has moved further from the wall, and the velocity gradient has been reduced below that observed closer to the element. Qualitatively the wakes are similar for different spacings; however, some differences are noted. If the rates of growth of the affected regions are compared by plotting the thickness δ_i of the internal boundary layer below the knees against the downstream distance x, the data are correlated approximately by

$$\frac{\delta_i}{R} = A \, \mathrm{Log}_e\left[\frac{X/H}{B}\right] \tag{9}$$

where A and B are tabulated in Table 4.

Table 4.

Coefficients for Equation (9)

S/H	∞	240	120	60	30
A	0.224	0.212	0.191	0.176	0.165
B	2.924	2.216	1.369	0.843	0.580

Clearly the rate of growth of δ_i depends on the spacing of the two roughness elements, and it decreases with decreased spacing in proportion to the value of the coefficient A. The effect of the coefficient B, however, is such as to cause δ_i to be larger initially for all second elements, and δ_i is increased by decreasing S/H.

Equation (1) shows that $\delta_i \simeq R$ at X/H = 250 for all spacings; i.e., plots of (1) converge at X/H = 250.

It is expected that the presence of the second element will affect the wake profiles of the first between the two elements, especially very close to the second. This deviation is shown in Fig. 12. In this figure the curves depict the longitudinal distribution of mean velocity in the wake of the single element at constant wall distance. The wall distance corresponding to the crest of the roughness element is y/R = 0.1049. The upstream points, as designated in the legend, refer to mean velocities between the two elements with the spacing S/H = 30, and at the X/H location measured from the upstream element. Thus "upstream" refers to the second element, but X/H refers to the first. On the other hand, the points designated as "downstream" are measured downstream of the second element. Thus, the figure shows the effect of the second element on the wake of the first and of the first element on the wake of the second.

The curves of Fig. 12 provide a picture of the velocity variation at several levels in the wake of a single element. The abrupt rise in velocity at the level nearest the wall indicates that the reattachment point is near X/H = 9. This agrees with the value determined from the distribution of the local skin friction coefficient. Velocities at y/R = 0.068 between two elements are fairly well predicted by the single element curve. Further from the wall, however, the velocities are higher between elements than behind a single element. Apparently retardation very near the wall between the two elements, resulting from blockage by the second element, is accompanied by higher core

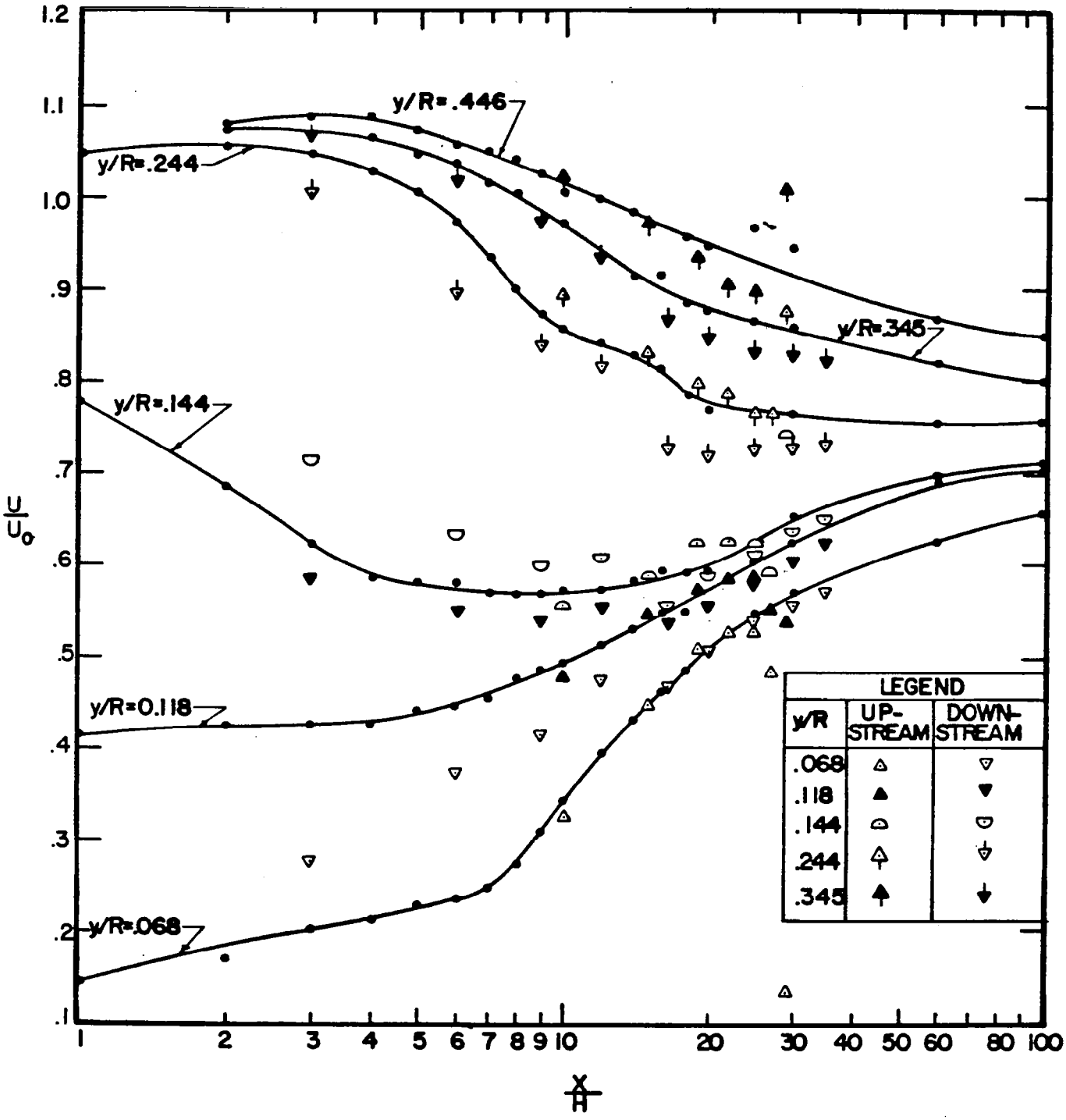

Fig. 12 Mean Velocity Distribution

velocities. The abrupt decrease in velocity observed near X/H = 30 for y/R = 0.068 and 0.118 is accompanied by a sudden rise in velocity at X/H = 30 at Y/R = 0.144 and higher levels. The latter departure from single-wake behavior shows that the single-element data could not be applied between elements too near to the second element.

Mean velocities downstream of the second element approach the single-element values after twenty or thirty element heights, and agreement is better further downstream. Close to the wall it is observed that velocities are much higher than single-element values. Agreement is better away from the wall, e.g., y/R = 0.345, but real merging of the one-element and two-element profiles occurs downstream of X/H = 35.

Velocity profiles for all spacings compare well with single-element wake profiles at X/H = 100, but complete merging occurs even further downstream. Wider spacing of elements than S/H = 30 results in better agreement with single-element wake profiles. However, complete agreement is not possible in the range of spacing used, since recovery of a fully developed flow condition does not occur for X/H < 240, as is seen in Fig. 7. Turbulence profiles are probably better indicators of the fully developed condition, or of departures from it. They will be presented next.

The turbulence, as well as the mean velocity, is affected by the first element. Figure 10 shows a comparison of longitudinal turbulence profiles as 15 element heights upstream of the second element for the five spacings considered. For S/H = 240 the upstream profile is at

X/H = 225 with respect to the first element. Comparison of it with the profile for the single element (S/H = ∞) indicates that even this upstream profile is slightly disturbed, although the fully developed distribution is approximated near the wall, i.e., $y/R < 0.3$. On the other hand, the disturbance has not reached the core region, $y/R > 0.5$, of the profile for the S/H = 30 spacing. Thus a wide variety of disturbed profiles are shown in this figure.

The response of the flow to the varied upstream conditions is also presented in Fig. 13 at 20 element heights downstream of the second element. Here it is observed that a merging of the profiles occurs for $y/R < 0.2$, although the turbulence is far from being in a fully developed, or equilibrium, state. The merging of profiles noted here progresses to $y/R = 0.24$ at X/H = 40 and to $y/R = 0.5$ at X/H = 100. The approximate locus of the merged points at X/H = 100 is shown in Fig. 13 as a dashed line. However, the dashed line does not approximate the fully developed profile shown at the left of Fig. 13. Thus the recovery is very slow indeed, even near the wall.

The influence of the downstream element on the turbulence is shown in Fig. 14. The open circles show normal turbulence decay behind a single element. The closed circles show the influence of the second element for the spacing S/H = 30. The turbulence level is reduced between the elements but rises to a slightly higher maximum behind the second element. Rates of decay of u' appear to be approximately the same for the single element, i.e., between the elements and behind the second element. The suppression of turbulence

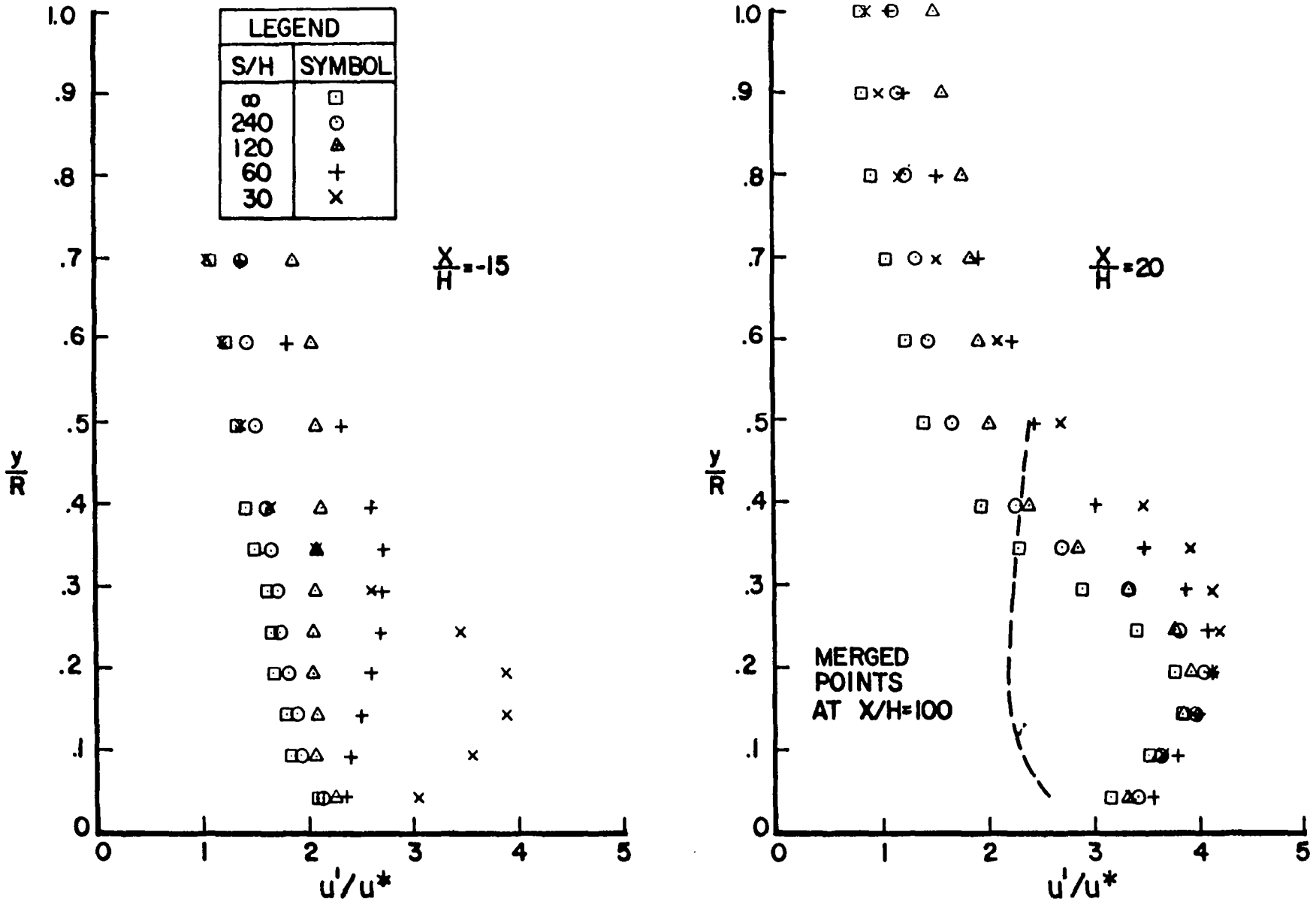

Fig. 13 Turbulence Profiles

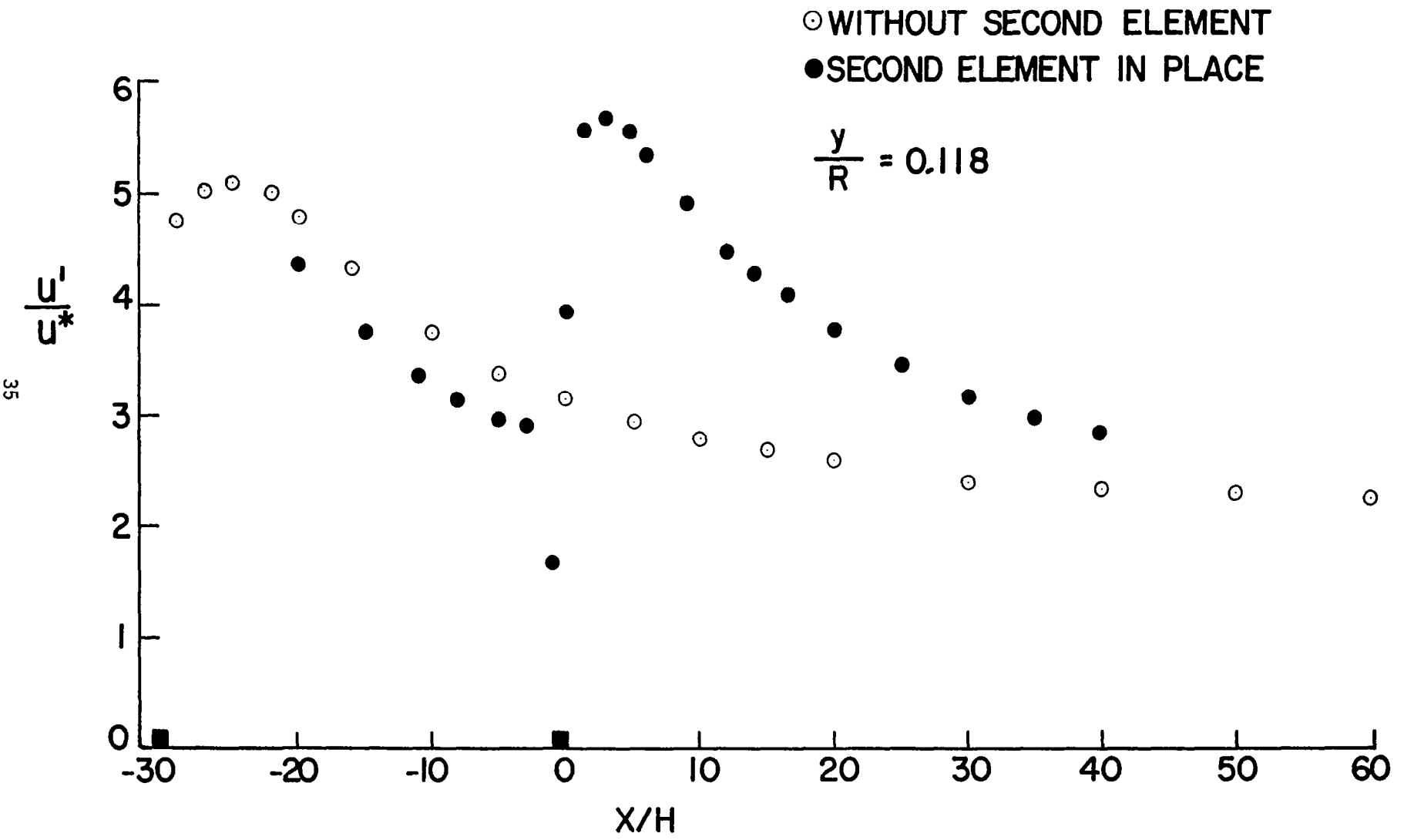

Fig. 14 Longitudinal Distribution of Turbulence Near the Wall

between the elements may be associated with the higher core velocities noted in Fig. 12. This would require lower production of turbulence at the element height. The situation appears to be reversed in the wake of the second element, where core velocities are lower, necessitating higher wall velocities with a concomitant increase of turbulence.

The curves of Fig. 15 show the distribution of longitudinal turbulence for the single-element wake at constant wall distance. The curves are observed to begin to rise significantly at the value of X/H corresponding to $y = \delta_i$, and these rise "points" can be predicted from (9). The maximum values of u' are achieved at $y < \delta_i$, but at a value of y still within the high velocity gradient portion of the flow, as may be verified by comparing the curve for y/R = 0.144 with the profiles of Fig. 10. All the curves of Fig. 15 merge at the right, forming virtually a single decay curve, the beginning "point" of which corresponds roughly with the "lower knee," or bend, of the profiles of Fig. 10. The velocity gradient and turbulence production below the lower knee is greatly reduced, thus allowing the decay of the excess turbulence energy to its equilibrium value.

The open points of Fig. 15 depict the u' distribution for S/H = 30 measured at three wall distances behind the second element. Higher turbulence levels (than for the single element) are observed immedicately behind the element and in the core region, reflecting undissipated, diffused upstream turbulence energy. However, the curves merge as before and approach single element values at X/H = 100.

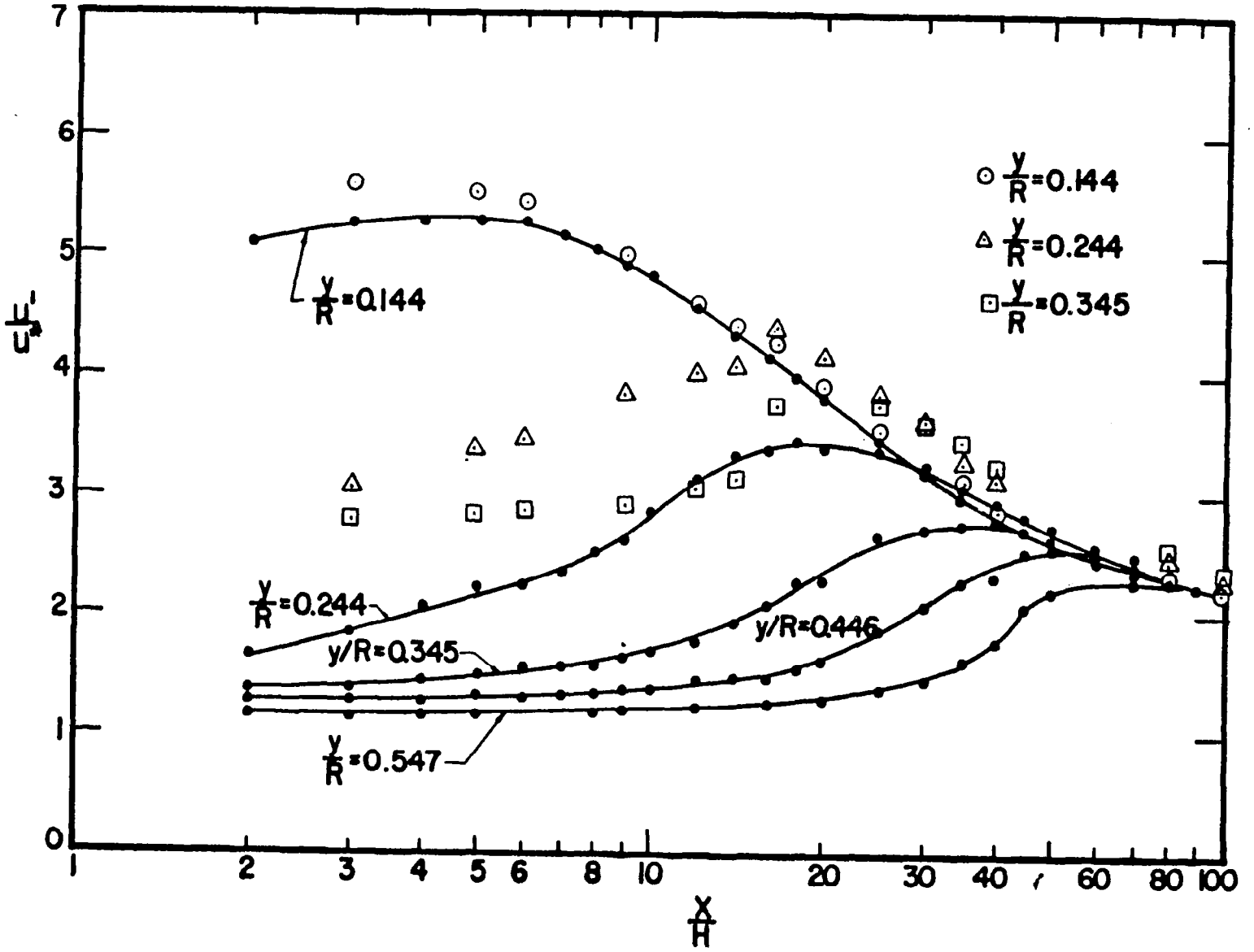

Fig. 15 Longitudinal Distribution of Turbulence

Reynolds shear stresses are shown as curves in Fig. 16 for the single-element wake and as open points for the second-element wake with S/H = 30. The stresses are raised to the highest values at y/R corresponding roughly to the element height. The region of high stress propagates away from the wall, diminishing in magnitude with increasing X/H, and the wall region is first to return to the equilibrium distribution. Equilibrium is nearly attained by 200 element heights downstream.

The above results can be interpreted to support the following model pertaining to the development of a rough-wall flow from an initially fully developed smooth-wall flow. The first element of a series of discrete equally spaced elements creates an internal boundary layer, the thickness of which determines the wall distance at any downstream station where turbulence stresses begin to rise. The high velocity gradient below this point generates large amounts of turbulence energy near the element but diminishes downstream, so that losses from diffusion and convection to the core determine a maximum turbulence level. Farther downstream the velocity gradients are further reduced by radial momentum transport, and decay of turbulence stress follows. Near the wall the decay proceeds rapidly, by virtue of small eddy dissipation, but core decay is much slower and turbulence maxima are achieved much farther downstream.

Subsequent elements create new internal boundary layers which grow more slowly but have thicker starting values. It is conjectured that the growth rate may decrease and the starting thickness

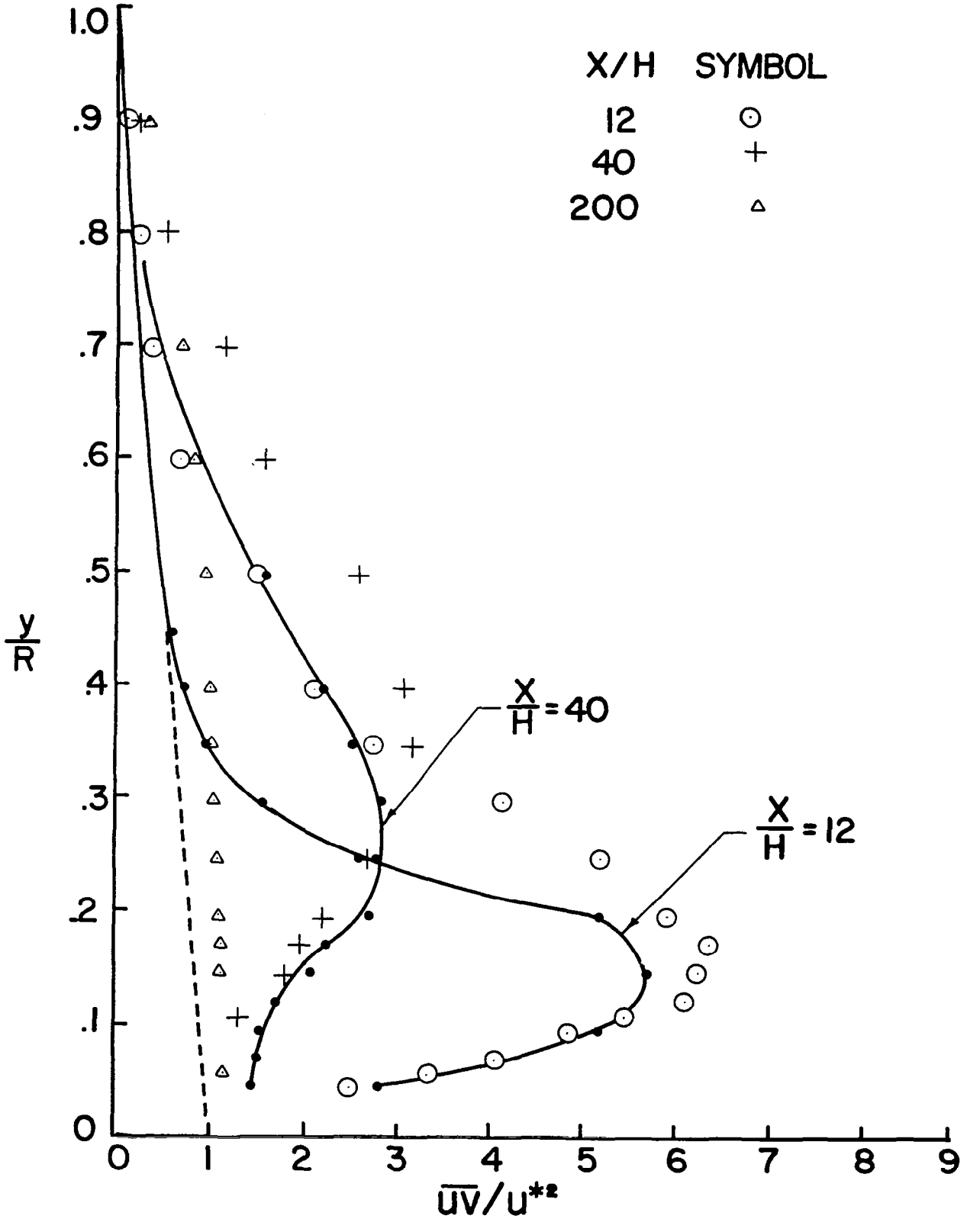

Fig. 16 Reynolds Shear Stress Profiles

increase monotonically with element number. In a flow over a surface artificially roughened with repeated-rib roughness, the latter extrapolation would imply the development of a "periodic" wall layer, in which the rise and fall of turbulence stress is observed, which supplies energy by diffusion to a contiguous core of stationary turbulence structure. The latter picture is that observed by Siuru and Logan in fully developed rough-wall flow.

Further experiments are necessary to verify the above model and, assuming that it can be verified, to determine the effect of element spacing and height on the thickness of the periodic wall layer.

CHAPTER 7

CONCLUSIONS

The present investigation leads to the conclusion that the integrated momentum flow close to the surface behind an obstacle can be greater than the upstream momentum flow, provided that the exponent of the upstream velocity profile is sufficiently high and that the boundary layer has been disturbed by upstream obstacles and is not in equilibrium. An additional effect is that the rise of turbulence level immediately behind the obstacle is also dependent on the profile exponent in a disturbed layer.

The development of Reynolds shear stress and turbulence intensity in the wake of an obstacle in a layer disturbed by upstream obstacles is shown to depend on the degree of disturbance as indicated by the power law exponent and to be contained within the internal boundary layer of thickness given by Eq. (9).

Flow over an obstacle in a disturbed layer is related to the smooth-rough wall transition through the model proposed in Chapter 6.

REFERENCES

Fichtl, G.H., D.W. Camp and W. Frost, 1977: Sources of low-level wind shear around airports. J. Aircraft, 14, 5-14.

Frost, W., and A.M. Shahabi, 1977: A field study over a simulated block building. NASA CR-2804, NASA/Marshall Space Flight Center, AL.

_____, G.H. Fichtl, J.R. Connell and M.L. Hutto, 1977: Mean horizontal wind profiles measured in the atmospheric boundary layer about a simulated block building. Bound-Layer Meteor., 11, 135-145.

Laufer, J., 1954: The structure of turbulence in fully developed pipe flow. NACA Rept. 1174.

Logan, E., and D.W. Camp, 1978: Preliminary comparison of model and prototype wakes. AIAA Paper No. 78-254.

Phataraphruk, P., and E. Logan, 1978: Response of a turbulent pipe flow to a single roughness element. Developments in Theoretical and Applied Mechanics, 9, 139-149.

_____, 1979: Turbulent pipe flow past a rectangular roughness element. Symposium on Turbulent Boundary Layers, ASME Bk. No. G00145, 187-196.

Rider, N.E., 1952: The effect of a hedge on the flow of air. Quart. J. Roy. Meteor. Soc., 78, 97-101.

Siuru, W.D., and E. Logan, 1977: Response of a turbulent pipe flow to a change in roughness. J. Fluids Eng., 99, 548-555.

Woo, H.G.C., J.A. Peterka and J.E. Cermak, 1977: Wind tunnel measurements in the wakes of structures. NASA CR-2806, NASA/Marshall Space Flight Center, AL.

1. REPORT NO.	2. GOVERNMENT ACCESSION NO.	3. RECIPIENT'S CATALOG NO.
NASA CR-3284		

4. TITLE AND SUBTITLE	5. REPORT DATE
Wake Characteristics of Buildings in Disturbed Boundary Layers	May 1980
	6. PERFORMING ORGANIZATION CODE
7. AUTHOR(S)	8. PERFORMING ORGANIZATION REPORT #
Earl Logan, Jr., and Jingfa Chang	
9. PERFORMING ORGANIZATION NAME AND ADDRESS	10. WORK UNIT NO.
College of Engineering and Applied Sciences Arizona State University Tempe, Arizona 85281	M-298
	11. CONTRACT OR GRANT NO. NAS8-32357
12. SPONSORING AGENCY NAME AND ADDRESS	13. TYPE OF REPORT & PERIOD COVERED
National Aeronautics and Space Administration Washington, D. C. 20546	Contractor Report
	14. SPONSORING AGENCY CODE

15. SUPPLEMENTARY NOTES

Final Report
Marshall Technical Monitors: Dennis W. Camp and Margaret B. Alexander

16. ABSTRACT

Measurements relevant to the effect of buildings on the low-level atmospheric boundary layer are presented. Field measurements of velocity and turbulence in the wake of a block building 3.2 m high and 26.8 m long are presented which show an apparent increase in momentum flow above the upwind value. The effect has been studied in a pipe flow apparatus in which a fully developed boundary layer is disturbed by a single roughness element or obstacle. A second element, simulating the building, is placed at various downstream distances from the first obstacle; and velocity and turbulence profiles, measured by constant-temperature hot-wire anemometer, are presented for regions upstream and downstream of the simulated building. Velocity-deficit and turbulence-excess decay characteristics of the disturbed or nonequilibrium layer are correlated with power law exponents and apparent roughness length at various distances downstream of the disturbance. Model wake profiles from the simulated building are compared at various stations for equilibrium and nonequilibrium upstream profiles. Empirical correlations relating building wake profiles to upstream nonequilibrium parameters are presented. The relationship of the data to the smooth-rough transition is discussed, and a flow model is presented.

17. KEY WORDS	18. DISTRIBUTION STATEMENT
Surface boundary layer Boundary flow Aircraft safety	Unclassified - Unlimited Subject Category 47

19. SECURITY CLASSIF. (of this report)	20. SECURITY CLASSIF. (of this page)	21. NO. OF PAGES	22. PRICE
Unclassified	Unclassified	50	$4.50

For sale by National Technical Information Service, Springfield, Virginia 22151

NASA-Langley, 1980